Investigation of carbon dioxide adsorption by nitrogen-doped carbons synthesized from cubic MCM-48 mesoporous silica

Young-Jung Heo, Minh-Uyen T. Le and Soo-Jin Park♣

Department of Chemistry, Inha University, Incheon 22212, Korea

Carbon dioxide (CO_2) is a component of the flue gas of power plants and automobile emissions. This gas is recognized as a primary greenhouse gas and is a presumed agent of climate change [1,2]. The drawbacks of the traditional MEA liquid method that is used for CO_2 capture include the requirement for heavy equipment, and the toxic, flammable, corrosive, and volatile nature of the process [3]. Therefore, CO_2 capture by means of adsorption in porous materials has received increasing attention because this method has proven to be superior than the conventional technologies in terms of the advantages associated with it. Compared to traditional processes, the convenient reversibility of adsorption on porous solid materials based on physisorption for the capture and release of CO_2 makes this technique a greener and more cost-efficient method. To date, a variety of solid-based materials have been intensively studied for gas adsorption, especially CO_2 capture, such as metal organic frameworks, covalent organic frameworks, zeolites, activated carbons, functionalized graphene, carbon molecular sieves, chemically modified mesoporous materials, etc [4-13]. Furthermore, the low concentration of CO_2 in flue gas (ca. 15%) requires selective separation from the large volume of other component gases, mainly N_2 [14]. Ideally, solid sorbents designed for CO_2 capture should offer reduced energy consumption for regeneration, greater capture capacity, stability, selectivity, ease of handling, reduced environmental impact, etc. Currently, there is significant interest in the development of solid carbon adsorbents that are capable of selectively adsorbing CO_2, because of their large surface area, porosity, abundance, cost efficiency, low density, fast adsorption kinetics, and high chemical and thermal stability [15-18]. Furthermore, these materials offer some advantages in terms of ease of handing, pore structure, and surface characteristics, as well as low-regeneration energy [19]. Therefore, carbon materials are currently considered attractive candidate sorbents for CO_2 capture in the development of alternate clean and sustainable energy technologies. Based on these strengths, increasing efforts have recently been devoted to the synthesis of element-doped porous carbons that combine the high porosity and unique properties of doped carbon frameworks. The MCM-48 templated carbons have a high porosity without activation usually required to develop an accessible porous structure. Nitrogen doping has earned particular distinction because of the enhanced surface polarity, electrical conductivity, and electron-donor tendency conferred to the mesoporous carbons by nitrogen incorporation, which enables their application in CO_2 capture, electric double-layer capacitors, fuel cells, catalysis, etc [20,21]. In the present study, we describe an alternate approach for the production of nitrogen-containing carbon materials with a cubic structure that facilitates CO_2 diffusion and capture.

Fig. 1a presents the low angle X-ray diffraction (XRD) pattern of MCM-48. The pattern exhibits several well-resolved peaks in the low-angle range of $2\theta = 2°–6°$, which can be indexed as the (211), (220), (420), and (332) diffraction peaks; this pattern corresponds to the cubic *Ia3d* space group [2,22]. In Fig. 1b high-angle XRD patterns, the synthesized carbon materials show two apparent peaks at around $2\theta = 25°$ and $44°$, which correspond to the (002) and (101) diffractions of the graphite structure, involving the hexagonal graphitic site and rhombohedral graphitic site, respectively [23]. Low-angle XRD patterns of the carbons synthesized with various amounts of pyrrole were acquired, as shown in Fig.
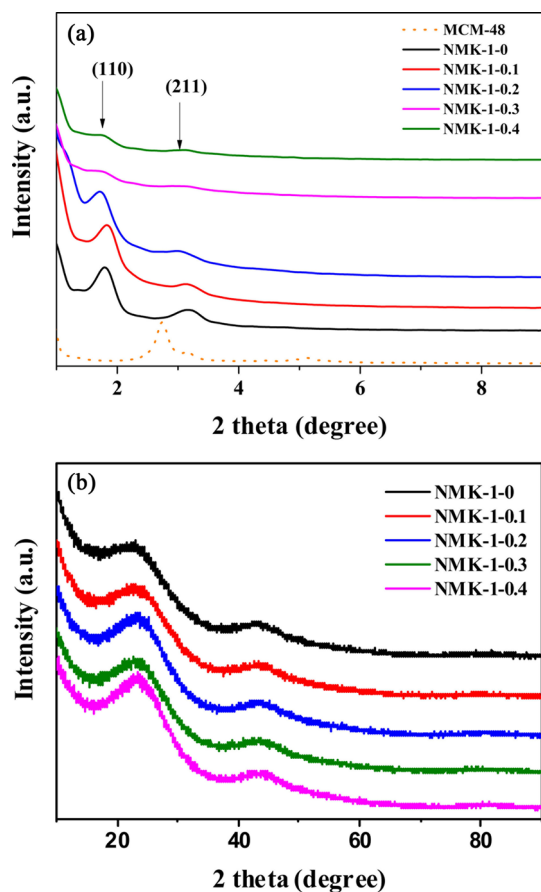
Fig. 1. (a) Low-angle and (b) High-angle X-ray diffraction patterns of carbons synthesized from MCM-48 with different amounts of pyrrole.
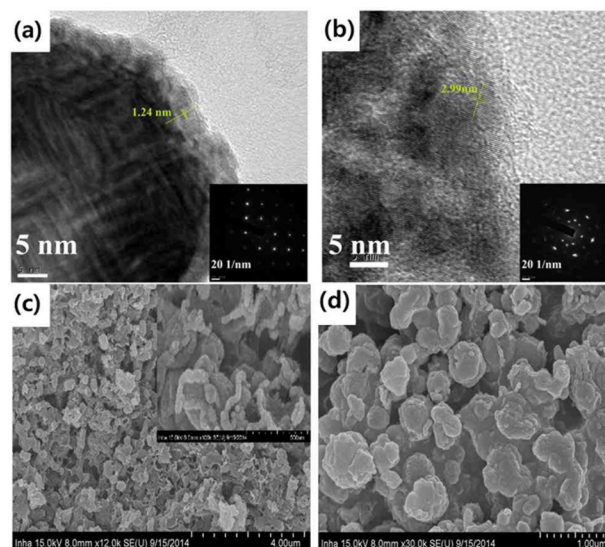

Fig. 2. Transmission electron microscopy images of (a) MCM-48 and (b) NMK-1-0.2. Scanning electron microscope images of (c) NMK-1-0 and (d) NMK-1-0.2.
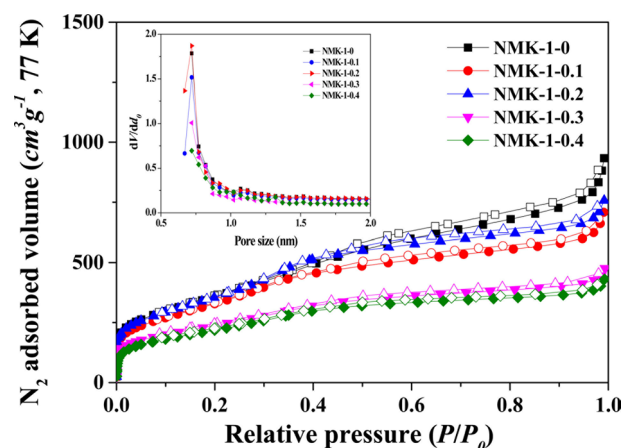

Fig. 3. Seventy-seven K/N₂ adsorption/desorption isotherms and micropore size distributions of the NMK-1 carbon materials.

1. The intense peaks at 2θ = 1.8° and 3.1° in the profiles of the synthesized carbon materials indicate long-range ordering of the highly ordered, uniform mesopores [24]. However, the structure of the resultant carbon material is different from that of the parent template MCM-48. Interestingly, the first intense (110) peak that was not observed for the MCM-48 template is apparent in the profile of the synthesized carbons; this is explained by proposing that the carbon networks were formed from two bicontinuous interconnected mesochannel systems of the MCM-48 structure (with *Ia3d* symmetry) constructed from two helical chains [25,26]. Due to the disconnectivity of the two sets of helix channels, 3D, cubic, bicontinuous, mesostructured replicas with two single-crystal nanowires that are periodically and helically twisted, which did not follow a simple replication of the template mesostructure-like, 2D hexagonally arranged pores, were generated [26]. In other words, the (110) peak is attributed to the phase transition of MCM-48 with *Ia3d* space group to a new cubic phase with *I*4₁32 space group, resulting from shrinkage of the carbon walls upon removal of the silica framework [24,27]. This change indicated that the structure of the synthesized carbon underwent a systematic transformation to a new ordered structure. Moreover, this peak was present in the XRD patterns of the other NMK-1 samples with a reduction of the intensity and a shift to higher 2θ angles as the amount of pyrrole used in the synthesis process increased. Transmission

electron microscopy (TEM) images of the MCM-48 template and the carbon materials are presented in Fig. 2a and b. The TEM image from the thin edges of the carbon particles shows that the carbon molecular sieve has a uniform pore distribution. The ordered cubic *Ia3d* mesostructure of MCM-48 can be seen in Fig. 2a. Furthermore, the TEM image of the inset in Fig. 2b indicates an ordered *I*4₁32 structure of NMK-1-0.2 after replication from the MCM-48 template (Fig. S1 and S2) [28]. Scanning electron microscopy demonstrated that the morphology of the NMK-1 porous carbons changed after the nitrogen-doping process using pyrrole (Fig. 2c and d).

Fig. 3 shows the nitrogen isotherms of the porous carbon matrixes obtained from the mesoporous silica MCM-48 template using pyrrole, as described above. The NMK-1-0 sample had a large specific surface area (about 1330 m² g⁻¹) and large primary pore volume (1.32 cm³ g⁻¹) (Table 1). Therefore, the nitrogen specific surface areas provided here are roughly estimated and the actual

Table 1. Seventy-seven K/N$_2$ adsorption/desorption isotherms and micropore size distributions of the NMK-1 carbon materials

Specimens	S_{BET}[a]	V_{Total}[b]	V_{Meso}[c]	V_{Micro}[d]	N-content[e]
	(m^2 g^{-1})	(cm^3 g^{-1})	(cm^3 g^{-1})	(cm^3 g^{-1})	(at%)
NMK-1-0	1326	1.42	1.32	0.10	-
NMK-1-0.1	1232	1.09	0.99	0.10	2.33
NMK-1-0.2	1323	1.16	1.07	0.09	3.28
NMK-1-0.3	865	0.72	0.61	0.11	3.75
NMK-1-0.4	808	0.65	0.57	0.08	3.55

[a]Specific surface area were calculated using Brunauer-Emmett-Teller equation in the relative pressure range of 0.1–0.3.
[b]Total pore volume estimated at a relative pressure P/P_0= 0.99.
[c]Mesopore volume (cm^3 g^{-1}): Barrett-Joyner-Halenda equation.
[d]Micropore volume (cm^3 g^{-1}): Dubinin-Radushkevich equation.
[e]Nitrogen content was measured by X-ray photoelectron spectroscopy.

specific surface areas are probably much closer to that reported before (about 1300 m^2 g^{-1}) on the basis of a nitrogen Brunauer-Emmett-Teller (BET) analysis. Further structural information was obtained by comparing the pore diameter of NMK with that of the silica wall thickness in MCM-48. The nitrogen adsorption/desorption isotherm and the corresponding pore size distribution for NMK-1-0 showed an inflection in the desorption curve, characteristic of capillary condensation within pores 3–4 nm in diameter, as shown in Table 1 and Fig. 3. The results of these nitrogen adsorption/desorption experiments are consistent with the data from the transmission electron microscopy analysis.

The pore diameter should be equal to the wall thickness of MCM-48 if the carbon synthesis simply followed a geometrical replication process. The silica wall thickness of MCM-48 was 1.24 nm, as determined from a TEM analysis of MCM-48 single crystals in Fig. 2a [29]. However, the pore diameter of the carbon replica was approximately twice the silica wall thickness in Fig. 2b. This difference demonstrated that structural transformation of the carbon frameworks took place upon removal of the silica wall. This structural transformation might be induced by strain in the carbon frameworks. A large contraction of the volume might also occur when pyrolysis of organic compounds to carbon takes place without external constraints. As shown in Fig. S3 micropores were present in the pore size distribution of all synthesized NMK-1-x carbons, where the pores created by the replicating process with diameters of about 0.72 nm were expected to facilitate diffusion of CO$_2$ inside the pore channels for effectively capturing CO$_2$.

Notably, a very intense, sharp peak at approximately 2.7 nm was observed(Fig. S3), indicating the formation of a highly uniform structure in the NMK-1-0.2 sample. The pore structure of NMK-1-0.2 seemed to be enhanced by the presence of the pyrrole reagent, and mesopores and micropores dominated the distribution profile of this sample compared to other samples. The CO$_2$ adsorption capacity of the porous carbons was investigated at 333.15 K (60°C) under flue gas conditions [30]. A comparative analysis of the CO$_2$ adsorption ability of the NMK samples is presented in Fig. 4a. The CO$_2$ capture performance of the samples, evaluated *via* the thermal gravimetric analysis (TGA) method under flue gas conditions, indicates that the nitrogen
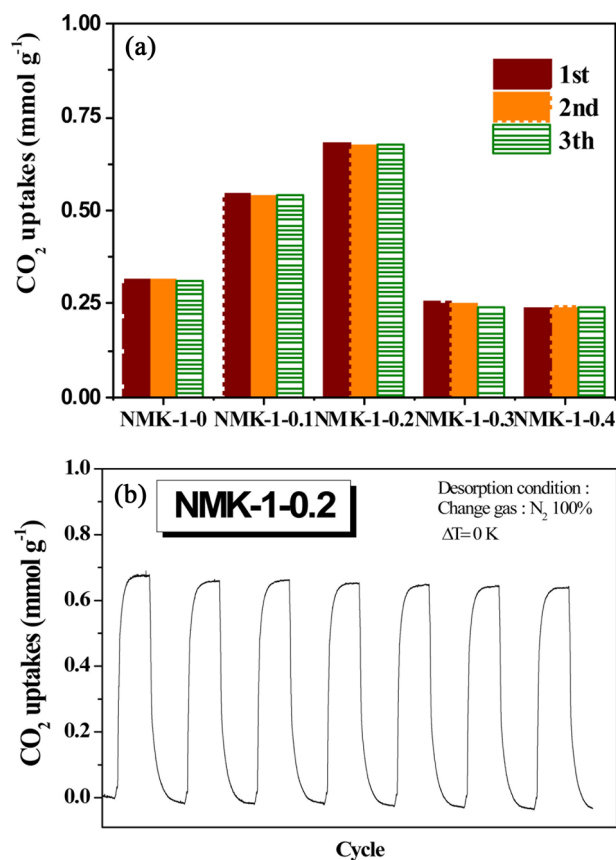

Fig. 4. (a) CO$_2$ uptakes of NMK materials at 333.15 K under flue condition and (b) CO$_2$ adsorption/desorption cycling test of NMK-1-0.2.

doping process using pyrrole significantly enhanced the CO$_2$ adsorption capacities of the NMK samples. It should also be noted that, although the NMK-1-0 sample (~1340 cm^3 g^{-1}, 0.31 mmol g^{-1} CO$_2$ uptakes) has a larger pore volume than the nitrogen-doped NMK carbons, the adsorption uptake of this sample is considerably lower than that of NMK-1-0.1 (with ~0.55 mmol g^{-1} CO$_2$ uptakes). This result demonstrates that the CO$_2$ adsorp-

tion capacity of the sorbents does not depend solely on textural properties such as the specific surface area or pore volume, but also on the pore size distribution as we previously reported for other carbons [13]. It is essential to bear this feature in mind when designing CO_2 carbon sorbents. Compared to NMK-1-0.1 (N: ~2.33 at%), the CO_2 adsorption capacity of the NMK-1-0.2 sample (N: ~3.75 at%) was significantly improved due to the higher nitrogen content on the surface. In this case, the CO_2 attraction ability of the nitrogen functional groups clearly contributed to enhancement of the CO_2 performance of the nitrogen-doped NMK carbons.

In contrast, the specific surface area and the porosity of NMK-1-x decreased notably when the pyrrole used in the synthesis process exceeded 0.3 g. To explain this trend, it was hypothesized that the observed degradation of the structural properties is a consequence of pyrrole polymerization outside of the MCM-48 pores [31]. Generally, the porosity of the resulting carbon materials is strongly dependent on the degree of template pore filling. After infiltration into the template pores, the carbon precursor undergoes polymerization. However, release of the carbon source from inside the template pores also occurs during polymerization. Deposition of the released precursor (sucrose and pyrrole) on the external template surface leads to non-porous carbon and consequently reduces the porosity of the carbon materials. Therefore, the CO_2 capture ability of NMK-1-0.3 and NMK-1-0.4 is two times less than that of NMK-1-0.2, even though the nitrogen deposited on the surfaces of the former is higher than that on the latter. Moreover, it is proposed that the nitrogen is mainly anchored on the external interface, resulting in lower CO_2 performance of these samples compared to NMK-1-0.2 and NMK-1-0.1 where the nitrogen functional groups are located in the pores. Regeneration of NMK-1-0.2, having the highest CO_2 sorption, was examined using a TGA Pyris (Perkin Elmer, Waltham, MA, USA) 1 instrument. Gas-cycling experiments were conducted at 60°C under dry conditions: 15% CO_2 in pure N_2, and pure N_2 for the desorption process at 100°C, respectively. The regeneration experiment indicated no significant decrease in the CO_2 adsorption capacity of NMK-1-0.2 after 8 cycles under these testing conditions in Fig. 4b. This indicates that NMK-1-0.2 exhibits high-capacity separation, requiring mild conditions for regeneration.

In this work, NMK-1-0.2 exhibits excellent CO_2 adsorption capacity of 0.68 mmol g^{-1} at 333.15 K (1 bar, 15% CO_2) and good regeneration performance. Thus, it is a promising adsorbent for energy-efficient CO_2 capture from post-combustion processes.

Mesoporous siliceous materials were prepared at room temperature following the typical procedure. First, 1.2 g of cetyltrimethylammonium bromide (CTAB) was dissolved in water (50 mL) and stirred at room temperature (30°C) until all the surfactant molecules had dissolved. After adding 25 mL of ethanol, the solution was stirred for 5 min at 30°C. A 6 mL liquid portion of aq. NH_3 (0.09 mol) was added, and the solution was stirred vigorously. Finally, 1.8 mL (8 mmol) of the silica precursor, tetraethyl orthosilicate (TEOS), was added and the mixture was stirred at 300 rpm for a further 4 h. The typical composition of the initial gel is 0.41 CTAB: 11 aq. NH_3: 1.0 TEOS: 53 ethanol: 344 H_2O. The obtained precipitate was filtered off and washed with deionized water several times. The obtained white powder was dried at room temperature overnight. The dried powder was calcined in static air at 550°C at a heating rate of 3°C min^{-1} and maintained at 550°C for 9 h to remove the surfactant molecules.

The nitrogen-doped mesoporous carbons are denoted as NMK-1. Carbonization experiments were performed with sucrose, sulfuric acid, and various amounts of pyrrole. Typically, the synthesis of NMK-1-x involved dissolution of 1.25 g sucrose, 0.2–1.2 g pyrrole, and 0.14 g H_2SO_4 in 5.0 g H_2O; this solution was then combined with 1 g MCM-48 [19,22]. The sucrose solution corresponded approximately to the maximum amount of sucrose and sulfuric acid that could be contained in the pores of 1 g MCM-48. The resultant mixture was dried in an oven at 100°C, and the oven temperature was subsequently increased to 160°C. After 6 h at 160°C, the MCM-48 silica containing the partially carbonized organic masses was added to an aqueous solution of 0.75 g sucrose, 0.08 g H_2SO_4, and 5.0 g H_2O. The resultant mixture was again dried at 100°C, and the oven temperature was subsequently increased to 160°C. The ultimately obtained black powder was heated to 800°C in an inert nitrogen atmosphere at a rate of 5°C/min, and the oven was maintained at this temperature for 2 h. The carbon-silica composite thus obtained was washed with a 1 M NaOH solution in 50% ethanol-50% H_2O twice at 90°C in order to dissolve the silica template completely. Removal of the silica template was also performed with HF solutions instead of NaOH. The carbon samples obtained after silica removal were filtered, washed with ethanol, and dried at 120°C. The synthesized samples were denoted as NMK-1-x, where x corresponds to the weight of pyrrole added in the reaction (from 0 to 0.4 g).

XRD analyses were carried out on a powder diffractometer (D2 PHASER, Bruker, Karlsruhe, Germany) with CuKα radiation (λ = 1.5406 Å). The textural properties of the synthesized samples were investigated using a gas adsorption analyzer (Belsorp-max, BEL Co., Japan). N_2 adsorption/desorption isotherms were measured at 77 K in liquid nitrogen baths. The specific surface areas and porous volumes were determined using the BET equation, as well as the Horvath-Kawazoe and Barrett-Joyner-Halenda methods.

A TGA was performed to evaluate the CO_2 adsorption performance under flue gas conditions, using a Pyris 1 TGA (Perkin Elmer) [33]. All gases were of 99.99% purity. All samples were outgassed for 5 h at 200°C under a N_2 flow to remove guest molecules from the pore system, and kept at 60°C for 20 min under a N_2 flow before starting the CO_2 adsorption measurement. The CO_2 adsorption process was conducted for 60 min at 60°C using 15% CO_2 in N_2 gas, and the desorption process was carried out at 100°C over 60 min.

Conflict of Interest

No potential conflict of interest relevant to this article was reported.

Acknowledgments

References

[1] D'Alessandro DM, Smit B, Long JR. Carbon dioxide capture: prospects for new materials. Angew Chem Int Ed, **49**, 6058 (2010). http://dx.doi.org/10.1002/anie.201000431.

[2] Armatas GS, Kanatzidis MG. Mesostructured germanium with cubic pore symmetry. Nature, **441**, 1122 (2006). http://dx.doi.org/10.1038/nature04833.

[3] Yang H, Xu Z, Fan M, Gupta R, Slimane RB, Bland AE, Wright I. Progress in carbon dioxide separation and capture: a review. J Environ Sci, **20**, 14 (2008). http://dx.doi.org/10.1016/S1001-0742(08)60002-9.

[4] Mishra AK, Ramaprabhu S. Polyaniline/multiwalled carbon nanotubes nanocomposite-an excellent reversible CO_2 capture candidate. RSC Adv, **2**, 1746 (2012). http://dx.doi.org/10.1039/C1RA00958C.

[5] Fracaroli AM, Furukawa H, Suzuki M, Dodd M, Okajima S, Gándara F, Reimer JA, Yaghi OM. Metal-organic frameworks with precisely designed interior for carbon dioxide capture in the presence of water. J Am Chem Soc, **136**, 8863 (2014). http://dx.doi.org/10.1021/ja503296c.

[6] Liu J, Thallapally PK, McGrail BP, Brown DR, Liu J. Progress in adsorption-based CO_2 capture by metal-organic frameworks. Chem Soc Rev, **41**, 2308 (2012). http://dx.doi.org/10.1039/C1CS15221A.

[7] Xie LH, Suh MP. High CO_2-capture ability of a porous organic polymer bifunctionalized with carboxy and triazole groups. Chem Eur J, **19**, 11590 (2013). http://dx.doi.org/10.1002/chem.201301822.

[8] Patel HA, Je SH, Park J, Chen DP, Jung Y, Yavuz CT, Coskun A. Unprecedented high-temperature CO_2 selectivity in N_2-phobic nanoporous covalent organic polymers. Nat Commun, **4**, 1357 (2013). http://dx.doi.org/10.1038/ncomms2359.

[9] Meng LY, Park SJ. Effect of heat treatment on CO_2 adsorption of KOH-activated graphite nanofibers. J Colloid Interface Sci, **352**, 498 (2010). http://dx.doi.org/10.1016/j.jcis.2010.08.048.

[10] Kim BJ, Lee YS, Park SJ. Novel porous carbons synthesized from polymeric precursors for hydrogen storage. Int J Hydrogen Energy, **33**, 2254 (2008). http://dx.doi.org/10.1016/j.ijhydene.2008.02.019.

[11] Le MUT, Lee SY, Park SJ. Preparation of characterization of PEI loaded MCM-41 for CO_2 capture. Int J Hydrogen Energy, **39**, 12340 (2014). http://dx.doi.org/10.1016/j.ijhydene.2014.04.112.

[12] Bae TH, Hudson MR, Mason JA, Queen WL, Dutton JJ, Sumida K, Micklash KJ, Kaye SS, Brown CM, Long JR. Evaluation of cation-exchanged zeolite adsorbents for post-combustion carbon dioxide capture. Energy Environ Sci, **6**, 128 (2013). http://dx.doi.org/10.1039/C2EE23337A.

[13] Park SJ, Kim KD. Adsorption behavior of CO_2 and NH_3 on chemically surface-treated activated carbons. J Colloid Interface Sci, **212**, 186 (1999). http://dx.doi.org/ 10.1006/jcis.1998.6058.

[14] Saleh M, Tiwari JN, Kemp KC, Yousuf M, Kim KS. Highly selective and stable carbon dioxide uptake in polyindole-derived microporous carbon materials. Environ Sci Technol, **47**, 5467 (2013). http://dx.doi.org/10.1021/es3052922.

[15] Lee J, Kim J, Hyeon T. Recent progress in the synthesis of porous carbon materials. Adv Mater, **18**, 2073 (2006). http://dx.doi.org/10.1002/adma.200501576.

[16] Park SJ, Kim BJ, Lee YS, Cho MJ. Influence of copper electroplating on high pressure hydrogen-storage behaviors of activated carbon fibers. Int J Hydrogen Energy, **33**, 1706 (2008). http://dx.doi.org/10.1016/j.ijhydene.2008.01.011.

[17] Heo YJ, Park SJ. Synthesis of activated carbon derived from rice husks for improving hydrogen storage capacity. J Ind Eng Chem, **31**, 330 (2015). http://dx.doi.org/10.1016/j.jiec.2015.07.006.

[18] Park SJ, Kim KD. Influence of activation temperature on adsorption characteristics of activated carbon fiber composites. Carbon, **39**, 1741 (2001). http://dx.doi.org/10.1016/S0008-6223(00)00305-5.

[19] Chumphongphan S, Filsø U, Paskevicius M, Sheppard DA, Jensen TR, Buckley CE. Nanoconfinement degradation in $NaAlH_4$/CMK-1. Int J Hydrogen Energy, **39**, 11103 (2014). http://dx.doi.org/10.1016/j.ijhydene.2014.05.087.

[20] Wang Y, Wang X, Antonietti M. Polymeric graphitic carbon nitride as a heterogeneous organocatalyst: from photochemistry to multipurpose catalysis to sustainable chemistry. Angew Chem Int Ed, **51**, 68 (2012). http://dx.doi.org/10.1002/anie.201101182.

[21] Wei J, Zhou D, Sun Z, Deng Y, Xia Y, Zhao D. A controllable synthesis of rich nitrogen-doped ordered mesoporous carbon for CO_2 capture and supercapacitors. Adv Funct Mater, **23**, 2322 (2013). http://dx.doi.org/10.1002/adfm.201202764.

[22] Lysenko ND, Shvets AV, Yaremov PS, Il'in VG. Effect of the conditions of the matrix carbonization of sucrose on the structure and adsorption properties of mesoporous carbon materials. Theor Exp Chem, **44**, 374 (2008). http://dx.doi.org/10.1007/s11237-009-9055-z.

[23] Lee SY, Yoo HM, Park SW, Park SH, Oh YS, Rhee KY, Park SJ. Preparation and characterization of pitch-based nanoporous carbons for improving CO_2 capture. J Solid State Chem, **215**, 201 (2014). http://dx.doi.org/10.1016/j.jssc.2014.03.038.

[24] Yoon SB, Kim JY, Yu JS. Synthesis of highly ordered nanoporous carbon molecular sieves from silylated MCM-48 using divinylbenzene as precursor. Chem Commun, **6**, 559 (2001). http://dx.doi.org/10.1039/B009691L.

[25] Yang H, Zhao D. Synthesis of replica mesostructures by the nanocasting strategy. J Mater Chem, **15**, 1217 (2005). http://dx.doi.org/10.1039/B414402C.

[26] Ryoo R, Joo SH, Kruk M, Jaroniec M. Ordered mesoporous carbons. Adv Mater, **13**, 677 (2001). http://dx.doi.org/10.1002/1521-4095(200105)13:9<677::AID-ADMA677>3.0.CO;2-C.

[27] Kruk M, Jaroniec M, Ryoo R, Joo SH. Characterization of ordered mesoporous carbons synthesized using MCM-48 silicas as templates. J Phys Chem B, **104**, 7960 (2000). http://dx.doi.org/10.1021/jp000861u.

[28] Jiao F, Yen H, Hutchings GS, Yonemoto B, Lu Q, Kleitz F. Synthesis, structural characterization, and electrochemical performance of nanocast mesoporous Cu-/Fe-based oxides. J Mater Chem A, **2**, 3065 (2014). http://dx.doi.org/10.1039/C3TA14111J.

[29] Carlsson A, Kaneda M, Sakamoto Y, Terasaki O, Ryoo R, Joo SH. The structure of MCM-48 determined by electron crystallography. J Electron Microsc (Tokyo), **48**, 795 (1999). http://dx.doi.org/10.1093/oxfordjournals.jmicro.a023751.

[30] Heo YJ, Park SJ. A role of steam activation on CO_2 capture and separation of narrow microporous carbons produced from cellulose fibers. Energy, **91**, 142 (2015). http://dx.doi.org/10.1016/j.energy.2015.08.033.

[31] Lu AH, Schüth F. Nanocasting: a versatile strategy for creating nanostructured porous materials. Adv Mater, **18**, 1793 (2006). http://dx.doi.org/10.1002/adma.200600148.